Three-Dimensional Metal–Graphene–Nanotube Multifunctional Hybrid Materials

Zheng Yan,[†,∥] Lulu Ma,[‡,∥] Yu Zhu,[†,∥,#] Indranil Lahiri,[§] Myung Gwan Hahm,[‡] Zheng Liu,[‡] Shubin Yang,[‡] Changsheng Xiang,[†] Wei Lu,[†] Zhiwei Peng,[†] Zhengzong Sun,[†] Carter Kittrell,[†,⊥] Jun Lou,[‡] Wonbong Choi,[§,×,*] Pulickel M. Ajayan,[†,‡,*] and James M. Tour[†,‡,⊥,*]

[†]Department of Chemistry, [‡]Department of Mechanical Engineering and Materials Science, and [⊥]Richard E. Smalley Institute for Nanoscale Science and Technology, Rice University, 6100 Main Street, Houston, Texas 77005, United States, [§]Nanomaterials and Devices Laboratory, Department of Mechanical and Materials Engineering, Florida International University, Miami, Florida 33174, United States, [#]Present address: Department of Polymer Science, the University of Akron, 170 University Circle, Akron, Ohio 44325-3909, and [×]Present address: Department of Materials Science and Engineering, University of North Texas, 1155 Union Circle #305310, Denton, Texas 76203-5017. [∥]These authors contributed equally to this work.

ABSTRACT Graphene was grown directly on porous nickel films, followed by the growth of controlled lengths of vertical carbon nanotube (CNT) forests that seamlessly emanate from the graphene surface. The metal–graphene–CNT structure is used to directly fabricate field-emitter devices and double-layer capacitors. The three-dimensional nanostructured hybrid materials, with better interfacial contacts and volume utilization, can stimulate the development of several energy-efficient technologies.

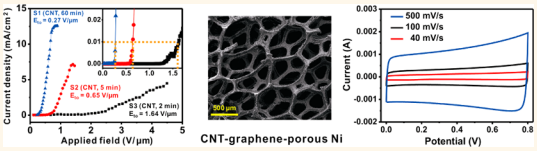

KEYWORDS: 3D · graphene · CNT · field-emitter device · capacitor · porous nickel

Carbon nanotubes (CNTs) grown directly on bulk metal substrates[1–5] used in several applications eliminate the need for post-transfer processes, but they suffer from inadequate CNT–metal-electrode contacts and low-surface-area-utilization efficiency. The use of graphene could bridge this gap and serve as an interfacial layer between metal and CNTs and enable new three-dimensional (3D) structures with better performance metrics. Here we report the direct growth of graphene on porous nickel films followed by the growth of controlled lengths of vertical CNT forests that seamlessly emanate from the graphene surface using our recently developed process[6] to form 3D hybrid structures. The metal–graphene–CNT structure is used directly to fabricate field-emitter devices and double-layer capacitors, demonstrating much improved performance over previously designed planar CNT–bulk metal structures.[4,5] The 3D nanostructured hybrid materials with better interfacial contacts and volume utilization can stimulate the development of several energy-efficient technologies.

Over the past decade, carbon nanotubes have been used in applications ranging from electronics to biotechnology.[4,7–17] In some devices, such as field-emitters and capacitors, the growth of the CNTs directly on the metal surfaces would eliminate further transfer process steps and improve the contact between the CNTs and the metal substrate. Recently, the techniques for directly growing CNTs on bulk metals have been developed and improved.[1–5] However, most present systems have inadequate CNT–metal interfacial contact and are inefficient in the surface area coverage. In this work, we present the direct growth of 3D CNT–graphene seamless hybrids on porous nickel substrates, where graphene serves as a linking agent between the CNT–metal interfaces so that the electrical power is used efficiently. In addition, the use of porous nickel films improves the surface-area-utilization efficiency of the metal substrates. In this research, the CNT–graphene–porous nickel structure has been used to fabricate field-emitter devices and double-layer capacitors without any post-transfer process being needed.

Figure 1 shows the procedures for the growth of CNT–graphene hybrids on porous nickel substrates. The porous nickel substrate

* Address correspondence to wonbong.choi@unt.edu, ajayan@rice.edu, tour@rice.edu.

Received for review April 10, 2012 and accepted November 29, 2012.

Published online November 29, 2012
10.1021/nn3015882

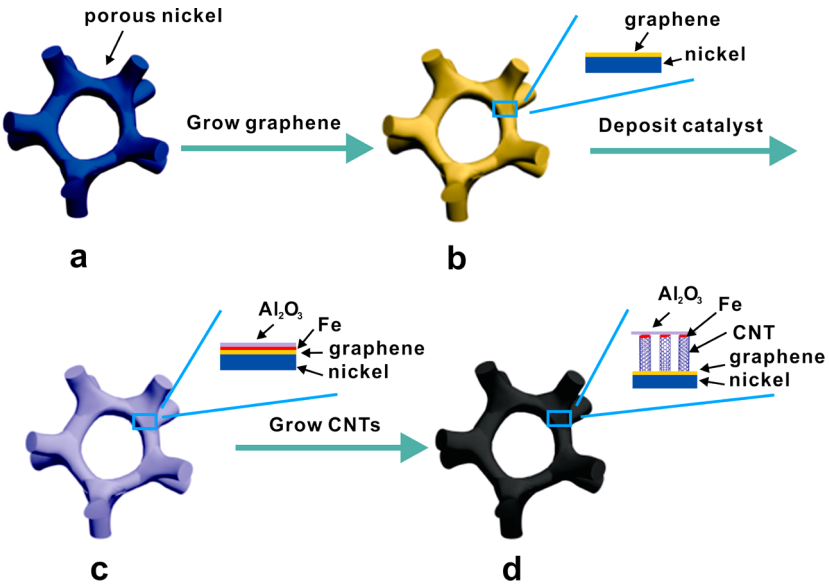

Figure 1. Scheme for the synthesis of CNT forests on graphene–porous nickel. (a) The porous nickel substrate. (b) Few-layer graphene is formed on the porous nickel by a CVD method. (c) Fe and Al_2O_3 are sequentially deposited on the graphene using e-beam evaporation. (d) A CNT forest is directly grown from the graphene surface while lifting the Fe/Al_2O_3 catalyst layer.

used in this research is a foam-like 1.2 mm thick nickel film, a widely used commercial battery material (Figure S1). Although the entire procedure can be done using a single layer of graphene,[6] in the optimal procedure here for devices, few-layer graphene was grown on the porous nickel films using a chemical vapor deposition (CVD) method.[18] The obtained graphene was characterized by Raman spectroscopy and transmission electron microscopy (TEM, Figure S2), demonstrating the few-layered structure and the high crystallinity[19–23] of the graphene. A 1.5 nm thick layer of catalytic Fe was deposited on the surface of the graphene using e-beam evaporation, followed by the deposition of a 10 nm thick Al_2O_3 as the buffer layer to ensure the catalytic activity of the Fe. Ethylene was used as the carbon source to grow CNTs at 750 °C. Water was also introduced during the CNT-growth process to remove amorphous carbon. Recently, other protocols have been published that combine CNTs and graphene.[24–27] However, using this protocol, the CNT forests raise the Fe/Al_2O_3 catalyst layer during the growth process while the vertically grown CNTs connect to the graphene layer through covalent bonds, leading to seamless high-quality CNT–graphene–metal interfaces.[6] The Fe/Al_2O_3 catalyst layer was deposited on both sides of the porous nickel films to increase the amount of CNTs attached to the substrates.

RESULTS AND DISCUSSION

Figure 2a shows optical images of porous nickel, graphene–porous nickel, and CNT–graphene–porous nickel, respectively. Scanning electron microscopy (SEM) images of CNTs grown on graphene–porous nickel are shown in Figure 2b–e. Figure 2b and c are the overviews of the as-grown 3D material, demonstrating an interconnected network structure. The surface region of Figure 2d is the Fe/Al_2O_3 catalyst layer that was lifted off during the growth of CNTs. Figure 2e shows the CNT–graphene interface, which is also an enlarged view of the CNT forests. The high-resolution transmission electron microscopy (HRTEM) image in Figure 2f indicates that most of the as-grown CNTs are single-walled, double-walled, or triple-walled, and the diameters are between 3 and 7 nm. The high degree of crystallinity of the CNTs was verified by Raman spectroscopy[4,28] in Figure 2g, showing a strong G peak at ~1580 cm^{-1} and a 2D peak at ~2620 cm^{-1}. The G/D ratio of the CNTs is ~3:1, suggesting the presence of few defects. The defects in CNTs are mainly sp^3 carbon atoms, which were introduced during the growth process and can be evaluated by the D peak.[28] The G peak arises from sp^2 carbon atoms in CNTs. Thus, comparing the ratio of intensities between the graphitic G peak and the defect-induced D peak is an efficient way to evaluate the quality of carbon nanotubes.[28] The strong radial breathing mode (RBM) signals in the inset of Figure 2g suggest that the diameters of the CNTs are small,[6] corresponding to the HRTEM observation. The 3D hybrid material is hydrophobic; the measured water contact angle was ~135°. After etching and removal of the porous nickel films using a mixture of HCl and $FeCl_3$, free-standing 3D CNT–graphene networks were obtained (Figure S3). The thickness of the sample decreased to ~0.8 mm from ~1.2 mm after the etching step. The CNTs bundled together due to the solvent-induced bundling effect (Figure S3b–d).[29] Throughout the etching process, CNTs were not washed away. This further confirmed that the CNTs were chemically attached to graphene. Ohmic contact at the junction

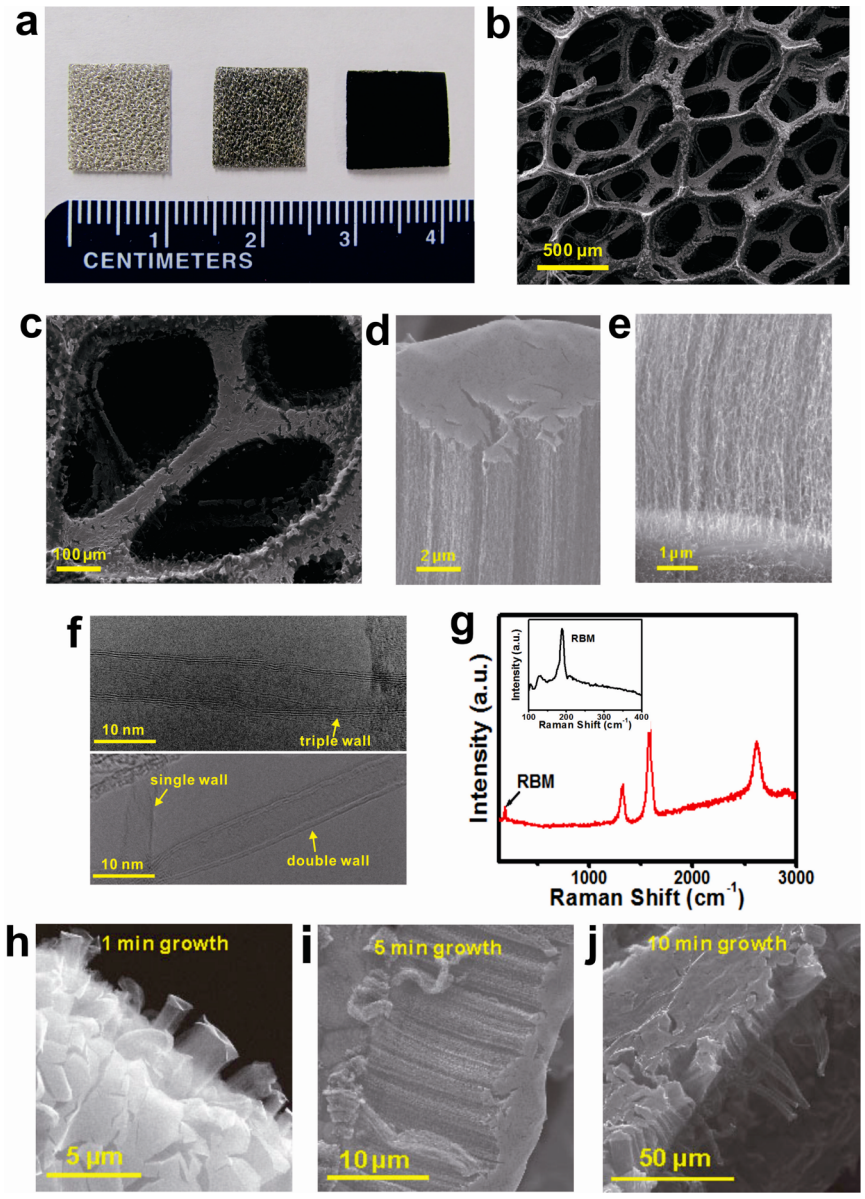

Figure 2. Characterization of CNT–graphene hybrids synthesized on porous nickel films. (a) Photographs of porous nickel, graphene–porous nickel, and CNT–graphene–porous nickel (from left to right). (b–e) SEM images of the same samples. The samples were synthesized using 1.5 nm Fe/10 nm Al_2O_3 as the catalyst, and the growth time was 10 min. (d) Side view of the CNT–catalyst interface, showing that the catalyst layer was raised up during the growth of CNTs. (e) Side view of CNT–graphene interface. (f) TEM images of the CNTs indicating the number of tube layers. (g) Raman spectra of the obtained CNTs under 633 nm excitation wavelengths. Inset: Spectra of the radial breathing modes (RBMs). (h–j) SEM images of obtained CNTs at different growth times. The samples were grown using 1.5 nm Fe/10 nm Al_2O_3 as the catalyst. The length of CNTs can be adjusted from ~3 μm to ~250 μm by changing growth time.

of the CNTs and graphene was observed,[6] suggesting a high-quality CNT–graphene interface. However, in most of the recently reported CNT–graphene hybrids,[30,31] the CNTs and graphene are physically combined and the poor junctions limit their potential applications in electronics and optics. Figure S4 shows the electrical properties of CNT–graphene hybrids. This identical electrical response from CNTs or graphene to the metal electrode indicates isotropic electrical properties.

The effects of the catalyst thickness and graphene on CNT growth were studied. For a convenient comparison, similar growth conditions were used to prepare the four samples shown in Figure S5a–d. Figure S5a–c are the SEM images of the samples grown on graphene–porous nickel films, separately using 0.5 nm Fe/3 nm Al_2O_3, 1 nm Fe/3 nm Al_2O_3, and 1.5 nm Fe/10 nm Al_2O_3 as the catalysts. Few CNTs were observed when the 0.5 nm thick Fe layer was used as the catalyst (Figure S5a). This is due to the rapid deactivation of the catalyst layer.[32] The problem was solved by increasing the thickness of the Fe layer from 0.5 nm to 1 nm (Figure S5b). However, when using 1 nm thick Fe as the catalyst, CNTs became bent during the growth process due to the instability of the Al_2O_3

catalyst layer. For well-aligned growth of CNTs on graphene–porous nickel, the optimized catalyst thickness was 1.5 nm thick Fe with 10 nm thick Al_2O_3 (Figure S5c). Figure S5d shows that it was difficult to grow the CNTs directly on the porous nickel without the graphene layer. Without graphene as the buffer layer on the nickel, the thin catalyst layer would likely deactivate due to alloying with nickel.

For some applications, the properties of the devices are closely related to the length of the CNTs. In this research, the CNT length can be controllably adjusted from 3 to 250 μm by changing the growth time (Figure 2h–j and Figure S6). Figure 2h–j show the SEM images of the obtained samples after separately growing for 1, 5, or 10 min using 1.5 nm Fe/10 nm Al_2O_3 as the catalysts. Figure 2h and Figure S6a,b show that the CNTs rapidly grow to ~3 μm in 1 min. After 5 and 10 min growth, the lengths of the CNTs were ~15 and ~35 μm, respectively (Figure 2i and j). If the growth time was further extended to 30 min, ~120 μm length CNTs were obtained (Figure S6c,d). However, during a 30 min growth, the catalyst layer broke and CNTs were bent due to losing support from the Al_2O_3 layer. After 60 min growth, the catalyst was still active and the length of obtained CNTs was ~250 μm (Figure S6e). If the growth time was extended to 120 min, no obvious change in CNT length was observed and much amorphous carbon was produced (Figure S6f). Apparently after 60 min of growth, the catalyst layer lost activity and the carbon sources were mainly transformed into amorphous carbon.

CNTs are known for their applications in field-emission devices.[4,5,7−13] In this research, we used the CNT–graphene–porous nickel to fabricate field-emission devices without needing any etching or post-transfer processing. As shown in Figure 3a, porous nickel serves as the cathode, graphene serves as the linking surface, CNTs are the field-emission emitters, and indium tin oxide (ITO)-coated glass is used as the anode. Figure 3b shows the test setup, and the inset in Figure 3b is an optical image of a field-emission device. Figure 3c presents the emission current density as a function of applied voltage in three different devices, S1 (CNT, 60 min), S2 (CNT, 5 min), and S3 (CNT, 2 min), which are, respectively, made using CNTs obtained after 60, 5, and 2 min of growth. The related lengths of CNTs are ~250, ~15, and ~7 μm. From Figure 3c, both the emission current density and the turn-on field are strongly affected by the CNT lengths. The device fabricated using 60 min of CNT growth had the best field-emission properties, the lowest turn-on field, and the highest emission current. The turn-on field for S1 (CNT, 60 min), measured at a current density of 0.01 mA/cm^2, is 0.26 V/μm, one of the lowest values reported.[4,5,7−13] For the same device, the current density at a field of 0.87 V/μm is 12.67 mA/cm^2, one of the highest reported values, to date.[4,5,7−13]

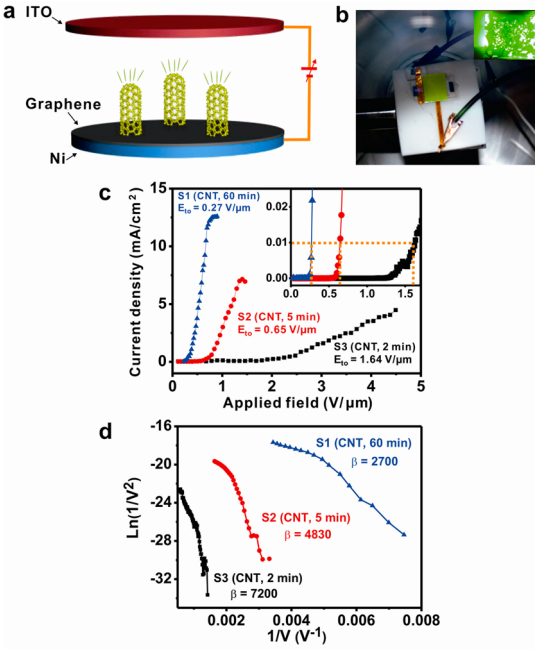

Figure 3. Field-emission characteristics of the CNT–graphene–porous nickel electrodes. (a) Schematic illustration of the field-emission setup. (b) Test setup for the field-emission devices. The inset in the upper right is the photograph of an emitting device. (c) Variation of the emission current density as a function of the applied field for S1 (CNT, 60 min), S2 (CNT, 5 min), and S3 (CNT, 2 min). The inset is the enlarged data, from which the turn-on fields are determined at the current density of 0.01 mA/cm^2. (d) Fowler–Nordheim plots obtained for S1 (CNT, 60 min), S2 (CNT, 5 min), and S3 (CNT, 2 min).

Fowler–Nordheim plots are shown in Figure 3d. At least two distinct slopes are observed in the plots, often seen in carbon nanotubes and attributed to a non-metal-like emission process from discrete energy states.[4] The corresponding field-enhancement factors (β) were estimated for high operation conditions from Fowler–Nordheim plots (Figure 3d), ranging from 2700 to 7200.

The emission properties are also related to the number of CNTs attached to the porous nickel through the graphene. When CNTs were grown on only one side of the porous nickel instead of both sides, the as-made device demonstrated poorer field-emission properties (sample CNT–graphene–porous nickel, blue curves in Figure S7) as compared to those of the device made by growing CNTs on both sides of the porous nickel (sample S2, CNT, 5 min, red curves in Figure 3c). The growth conditions for these two samples were the same. Surprisingly, pristine porous nickel also showed some field-emission responses (black curves in Figure S7). Nickel nanowires are known for their field-emission properties;[33] hence, porous nickel surface protrusions may be the source of the field emission. After coating the porous nickel with graphene, better field-emission properties were observed (red curves in Figure S7). However, the contributions of

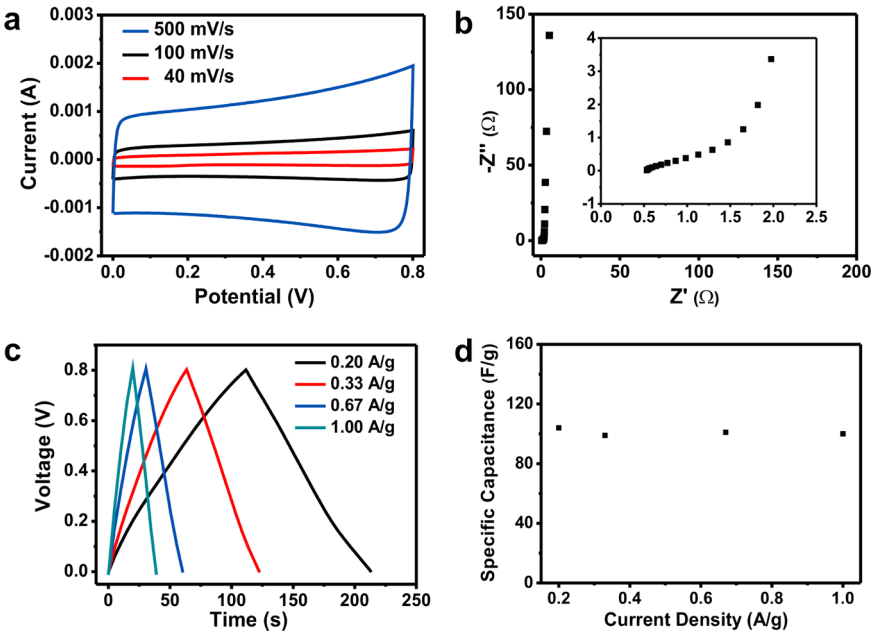

Figure 4. Double-layer capacitor performances of the devices fabricated using CNT–graphene–porous nickel. (a) CV curves for different scan rates. The rectangular shapes indicate the capacitive behavior. (b) Nyquist plot, showing the imaginary part *versus* the real part of impedance. Inset shows the data at high-frequency ranges. (c) Galvanostatic charge/discharge curves of CNT–graphene–porous nickel-based double-layer capacitor measured in the 6 M KOH electrolyte under different constant currents. (d) Various specific capacitance *versus* discharging current density. The device was made by 2 min growth CNTs on graphene–porous nickel.

the porous nickel and the graphene to the field-emission response of CNT–graphene–porous nickel samples are almost negligible in the applied field regime of the field-emission test here. Hence the CNT–graphene–metal hybrid is indeed unique in its functionality.

To demonstrate the high quality of the CNT–graphene–porous nickel contact interface, the capacitive properties were measured (Figure 4). Porous nickel was used as the current collector to fabricate an electrochemical double-layer capacitor (EDLC) without the need of any post-transfer or postetching processes. Aqueous KOH (6 M) was used as the electrolyte in the measurements. Figure 4 demonstrates that the EDLC made by this CNT–graphene–porous nickel structure exhibited excellent double-layer electrochemical performance and high rate performance. Figure 4a shows the cyclic voltammograms (CVs) of the EDLC at different scan rates. With an increase in scan rate, the current response increased accordingly, without any significant changes in the shape of the CV curve, indicating a good rate performance. The rectangular and symmetric shape of the CVs was also observed at high scan rates of 500 mV/s, supporting the suggestion of low contact resistance for the CNT–graphene–porous nickel interface.[4,34,35]

Figure 4b is the Nyquist plot based on a frequency response analysis of the frequency range from 1 MHz to 10 mHz. The Nyquist plot is almost a vertical line, indicating a nearly ideal capacitive behavior of the EDLC. The inset in Figure 4b is the magnified data in the high-frequency range, and the obvious transition between the semicircle and the migration of electrolyte corresponds to a resistance of 1.25 Ω. Figure 4c shows the galvanostatic charge–discharge curves at four different current densities. The specific capacitance was calculated from the discharge curves with values of 104, 99, 101, and 100 F/g obtained at current densities of 0.2, 0.33, 0.67, and 1.00 A/g, respectively (Figure 4d). The almost constant specific capacitance as the scan rate increased up to 1.00 A/g indicates the high diffusion conductivity of the active material and the electrolyte. Meanwhile, the calculated value is about 5 times higher than that of the EDLC fabricated by directly growing CNTs on Inconel without graphene as the linking surface[4] and is also comparable with the best recently reported values of the EDLC made with graphene oxide.[36–38]

In this research, we demonstrated the applications of pristine CNT–graphene–porous nickel in field-emission emitters and supercapacitors. If additives could be further introduced into graphene and CNTs during the growth process, such as by nitrogen doping, the doped hybrid material should also have potential applications in fuel cells and lithium batteries.[39,40]

CONCLUSION

In conclusion, we have shown the controlled growth of 3D CNT–graphene seamless hybrids on porous nickel substrates. This metal–graphene–nanotube structure overcomes several obstacles that previously hindered the further applications of CNTs, including inadequate CNT–metal–electrode contact, low

surface-area-utilization efficacy of bulk metals, and post-transfer difficulties. High-performance field-emission and double-layer capacitor properties were observed for these new 3D structures.

METHODS

Synthesis of 3D CNT–Graphene Hybrids on Porous Nickel. The porous nickel was received from Heze Tianyu Technology Development Company. The thickness was 1.2 mm, and the areal density was 320 g/m^2. Graphene was grown using the recently reported chemical vapor deposition method.[18] The catalyst (1.5 nm Fe) and buffer layer (10 nm Al_2O_3) were deposited in series on the graphene-covered porous nickel by e-beam evaporation. The growth of the CNTs was done at atmospheric pressure. The flow rates of ethylene, hydrogen, and argon were 100, 400, and 500 sccm, respectively. Hydrogen was used as the carrier gas to introduce water vapor into the system at a hydrogen flow rate of 10 sccm.[41] The assembled sample was annealed in the furnace under the same environment at 750 °C for 3 min before the carbon source was introduced. The growth time depended on the CNT forest height that was sought. Typically, a 10 min growth produced a CNT forest with a height of ~35 μm. The deposited Al_2O_3 is an amorphous thin film. Thus, ethylene could diffuse through Al_2O_3 to contact Fe. At the beginning of CNT growth, Fe partially etched graphene under the hydrogen atmosphere and high temperature,[42] introducing some defects in the graphene film and then leading to the seamless growth of CNTs emanating from graphene.

Field-Emission Characterizations. Field-emission response of the samples was characterized in a custom-developed system, at a vacuum level of 10^{-7} Torr. Test setup for all the samples consisted of a parallel plate diode configuration, where CNT–graphene–porous nickel samples were made as the cathode and a flattened pure Cu sheet (99.99% purity and 0.6 mm thick) was used as the anode. The Cu sheet used as the anode was rectangular and twice the size of the cathode to ensure that all emitted electrons are collected by the anode. The distance between the anode and the top surface of the CNT–graphene–porous nickel substrate was 650 μm. Direct current voltage and current measurements involved a Keithley 248 high-voltage supply and 2010 digital multimeter, respectively. Field-emission tests in pulsed mode were conducted using an Agilent function generator (model 33220A) to generate an electrical field, attached to a Trek high-voltage amplifier (model 20/20C), and the current was measured through a Pearson current monitor (model 4100, having 1.0 V/A), coupled with an Agilent oscilloscope (model MSO6034A). A sine-wave function was applied through the function generator, and the frequency of the pulsed signal was kept constant at 1 kHz for all the tests. While capturing emission images from the devices, a green phosphor-coated ITO glass replaced the flattened Cu sheet as the anode.

Double-Layer Capacitor Characterizations. The capacitance measurements were studied in a two-electrode system using 6 M KOH solution as the electrolyte. The as-grown CNT–graphene–porous nickel structure (1 × 1 cm) was directly tested as the electrode. Galvanostatic charge–discharge measurements were done using Arbin instruments BT2043. The cyclic voltammetry and electrochemical impedance spectroscopy were done using an Autolab workstation (PGSTAT302N). The equation $C = 2(I/m) \times (dt/dV)$ was used to calculate the specific capacitance from the slope of the charge–discharge curves (dV/dt), where I is the applied current and m is the mass of each electrode. The amount of active materials was determined by measuring the masses of hybrid materials before and after graphene and CNT growth using a microbalance (CAHN, C-31).

Other Characterizations. The Raman spectra were recorded with a Renishaw Raman RE01 scope using a 633 nm excitation argon laser. SEM images were taken using a FEI Quanta 400 field-emission gun scanning electron microscope. TEM images were taken using a 200 kV JEOL FE2100 transmission electron microscope.

Conflict of Interest: The authors declare no competing financial interest.

Acknowledgment. The authors thank J. Lin and C. Zhang for valuable discussions. The ONR MURI program (#00006766, N00014-09-1-1066), AFOSR MURI (FA9550-12-1-0035), Lockheed Martin LANCER IV Program, and AFOSR (FA9550-09-1-0581 and FA9550-09-1-0544) provided funding.

Supporting Information Available: SEM images and optical images of porous nickel and CNT–graphene–porous nickel, electronic properties of graphene–CNT, and field-emission properties of CNT–graphene–porous nickel, graphene–porous nickel, and porous nickel. This material is available free of charge *via* the Internet at http://pubs.acs.org.

REFERENCES AND NOTES

1. Wang, B.; Liu, X.; Liu, H.; Wu, D.; Wang, H.; Jiang, J.; Wang, X.; Hu, P.; Liu, Y.; Zhu, D. Controllable Preparation of Patterns of Aligned Carbon Nanotubes on Metals and Metal-coated Silicon Substrates. *J. Mater. Chem.* **2003**, *13*, 1124–1126.
2. Ng, T. H.; Chen, B.; Koehne, J. E.; Cassell, A. M.; Li, J.; Han, J.; Meyyappan, M. Growth of Carbon Nanotubes: A Combinatorial Method to Study the Effects of Catalysts and Under Layers. *J. Phys. Chem. B* **2003**, *107*, 8484–8489.
3. Xu, F.; Liu, X.; Tse, S. D. Synthesis of Carbon Nanotubes on Metal Alloy Substrates with Voltage Bias in Methane Inverse Diffusion Flames. *Carbon* **2006**, *44*, 570–577.
4. Talapatra, S.; Kar, S.; Pal, S. K.; Vajtai, R.; Ci, L.; Victor, P.; Shaijumon, M. M.; Kaur, S.; Nalamasu, O.; Ajayan, P. M. Direct Growth of Aligned Carbon Nanotubes on Bulk Metals. *Nat. Nanotechnol.* **2006**, *1*, 112–116.
5. Lahiri, I.; Seelaboyina, R.; Hwang, J. Y.; Banerjee, R.; Choi, W. Enhanced Field Emission From Multi-Walled Carbon Nanotubes Grown on Pure Copper Substrate. *Carbon* **2010**, *48*, 1531–1538.
6. Zhu, Y.; Li, L.; Zhang, C.; Casillas, G.; Sun, Z.; Yan, Z.; Ruan, G.; Peng, Z.; Raji, A.-R. O.; Kittrell, C.; *et al*. A Seamless Three-Dimensional Carbon Nanotube Graphene Hybrid Material. *Nat. Commun.* **2012**, 10.1038/ncomms2234.
7. Fan, S.; Chapline, M. G.; Franklin, N. R.; Tombler, T. W.; Cassell, A. M.; Dai, H. Self-oriented Regular Arrays of Carbon Nanotubes and Their Field Emission Properties. *Science* **1999**, *283*, 512–514.
8. Jo, S. H.; Huang, J. Y.; Chen, S.; Xiong, G. Y.; Wang, D. Z.; Ren, Z. F. Field Emission of Carbon Nanotubes Grown on Carbon Cloth. *Appl. Phys. Lett.* **2004**, *85*, 810–812.
9. Jung, Y. J.; Kar, S.; Talapatra, S.; Soldano, C.; Viswanathan, G.; Li, X.; Yao, Z.; Ou, F. S.; Avadhanula, A.; Vajtai, R.; *et al*. Aligned Carbon Nanotube-Polymer Hybrid Architectures for Diverse Flexible Electronic Applications. *Nano Lett.* **2006**, *6*, 413–418.
10. Sveningsson, M.; Morjan, R. E.; Nerushev, O. A.; Campbell, E.; Malsch, D.; Schaefer, J. A. Highly Efficient Electron Field Emission from Decorated Multiwalled Carbon Nanotube Films. *Appl. Phys. Lett.* **2004**, *85*, 4487–4489.
11. Bonard, J. M.; Salvetat, J. P.; Stockli, T.; de Heer, W. A.; Forro, L.; Chatelain, A. Field Emission From Single-Wall Carbon Nanotube Films. *Appl. Phys. Lett.* **1998**, *73*, 918–920.
12. Lee, D. H.; Kim, J. E.; Han, T. H.; Hwang, J. W.; Jeon, S.; Choi, S. Y.; Hong, S. H.; Lee, W. J.; Ruoff, R. S.; Kim, S. O. Versatile Carbon Hybrid Films Composed of Vertical Carbon Nanotubes Grown on Mechanically Compliant Graphene Films. *Adv. Mater.* **2010**, *22*, 1247–1252.
13. Choi, W. B. Fully Sealed, High-Brightness Carbon Nanotube Field Emission Display. *Appl. Phys. Lett.* **1999**, *75*, 3129.
14. Cao, A.; Veedu, V. P.; Li, X.; Yao, Z.; Ghasemi-Nejhad, M. N.; Ajayan, P. M. Multifunctional Brushes Made from Carbon Nanotubes. *Nat. Mater.* **2005**, *4*, 540–545.

15. Teo, K. B. K.; Minoux, E.; Hudanski, L.; Peauger., F.; Schnell, J.-P.; Gangloff, L.; Legagneux, P.; Dieumegard, D.; Amaratunga, G. A. J.; Milne, W. I.; *et al*. Microwave Devices: Carbon Nanotubes as Cold Cathodes. *Nature* **2005**, *437*, 968.
16. Jarillo-Herrero, P.; van Dam, J. A.; Kouwenhoven, L. P. Quantum Supercurrent Transistors in Carbon Nanotubes. *Nature* **2006**, *439*, 953–956.
17. Lipomi, D. J.; Vosgueritchian, M.; Tee, B.; Hellstrom, S. L.; Lee, J. A.; Fox, C. H.; Bao, Z. Skin-Like Pressure and Strain Sensors Based on Transparent Elastic Films of Carbon Nanotubes. *Nat. Nanotechnol.* **2011**, *6*, 788–792.
18. Chen, Z.; Ren, W.; Gao, L.; Liu, B.; Pei, S.; Cheng, H. M. Three-Dimensional Flexible and Conductive Interconnected Graphene Networks Grown by Chemical Vapor Deposition. *Nat. Mater.* **2011**, *10*, 424–428.
19. Reina, A.; Jia, X.; Ho, J.; Nezich, D.; Son, H.; Bulovic, V.; Dresselhaus, M. S.; Kong, J. Large Area, Few-Layer Graphene Films on Arbitrary Substrates by Chemical Vapor Deposition. *Nano Lett.* **2009**, *9*, 30–35.
20. Li, X.; Cai, W.; An, J.; Kin, S.; Nah, J.; Yang, D.; Piner, R.; Celamakanni, A.; Jung, I.; Tutuc, E.; *et al*. Large-Area Synthesis of High-Quality and Uniform Graphene Films on Copper Foils. *Science* **2009**, *324*, 1312–1314.
21. Kim, K. S.; Zhao, Y.; Jang, H.; Lee, S. Y.; Kim, J. M.; Kim, K. S.; Ahn, J.-H.; Kim., P.; Choi, J.-Y.; Hong, B. H.; *et al*. Large-Scale Pattern Growth of Graphene Films for Stretchable Transparent Electrodes. *Nature* **2009**, *457*, 706–710.
22. Sun, Z.; Yan, Z.; Yao, J.; Beitler, E.; Zhu, Y.; Tour, J. M. Growth of Graphene from Solid Carbon Sources. *Nature* **2010**, *468*, 549–552.
23. Yan, Z.; Peng, Z.; Sun, Z.; Yao, J.; Zhu, Y.; Liu, Z.; Ajayan, P. M.; Tour, J. M. Growth of Bilayer Graphene on Insulating Substrates. *ACS Nano* **2011**, *5*, 8187–8192.
24. Paul, R. K.; Ghazinejad, M.; Penchev, M.; Lin, J.; Ozkan, M.; Ozkan, C. S. Synthesis of a Pillared Graphene Nanostructure: a Counterpart of Three-Dimensional Carbon Architectures. *Small* **2010**, *6*, 2309–2313.
25. Jousseaume, V.; Cuzzocrea, J.; Bernier, N.; Renard, V. Few Graphene Layers/Carbon Nanotube Composites Grown at Complementary-Metal-Oxide-Semiconductor Compatible Temperature. *Appl. Phys. Lett.* **2011**, *98*, 123103–123103.
26. Zhang, L. L.; Xiong, Z.; Zhao, X. S. Pillaring Chemically Exfoliated Graphene Oxide with Carbon Nanotubes for Photocatalytic Degradation of Dyes under Visible Light Irradiation. *ACS Nano* **2010**, *4*, 7030–7036.
27. Fan, Z.; Yan, J.; Zhi, L.; Zhang, Q.; Wei, T.; Feng, J.; Zhang, M.; Qian, W.; Wei, F. A Three-Dimensional Carbon Nanotube/Graphene Sandwich and Its Application as Electrode in Supercapacitors. *Adv. Mater.* **2010**, *22*, 3723–3728.
28. Dresselhaus, M. S.; Dresselhaus, G.; Saito, R.; Jorio, A. Raman Spectroscopy of Carbon Nanotubes. *Phys. Rep.* **2005**, *409*, 47–99.
29. Futaba, D. N.; Hata, K.; Yamada, T.; Hiraoka, T.; Hayamizu, Y.; Kakudate, Y.; Tanaike, S.; Hatori, H.; Yumura, M.; Iijima, S.; *et al*. Shape-Engineerable and Highly Densely Packed Single-Walled Carbon Nanotubes and Their Application as Super-Capacitor Electrodes. *Nat. Mater.* **2006**, *5*, 987–994.
30. Das, S.; Seelaboyina, R.; Verma, V.; Lahiri, I.; Hwang, J. Y.; Banerjee, R.; Choi, W. Synthesis and Characterization of Self-organized Multilayered Graphene-Carbon Nanotube Hybrid Films. *J. Mater. Chem.* **2011**, *21*, 7289–7295.
31. Zhu, X.; Ning, G.; Fan, Z.; Gao, J.; Xu, C.; Qian, W.; Wei, F. One-Step Synthesis of a Graphene-Carbon Nanotube Hybrid Decorated by Magnetic Nanoparticles. *Carbon* **2012**, *50*, 2764–2771.
32. Helveg, S.; Lopez-cartes, C.; Sehested, J.; Hansen, P. L.; Clausen, B. S.; Rostrup-Nielsen, J. R.; Abild-pedersen, F.; Norskov, J. K. Atomic-Scale Imaging of Carbon Nanofibre Growth. *Nature* **2004**, *427*, 426–429.
33. Joo, J.; Lee, S. J.; Park, D. H.; Kim, Y. S.; Lee, Y.; Lee, C. J.; Lee, S. R. Field Emission Characteristics of Electrochemically Synthesized Nickel Nanowires with Oxygen Plasma Post-Treatment. *Nanotechnology* **2006**, *17*, 3506–3511.
34. Kaempgen, M.; Chan, C. K.; Ma, J.; Cui, Y.; Gruner, G. Printable Thin Film Supercapacitors Using Single-Walled Carbon Nanotubes. *Nano Lett.* **2009**, *9*, 1872–1876.
35. Du, C.; Yeh, J.; Pan, N. High Power Density Supercapacitors Using Locally Aligned Carbon Nanotube Electrodes. *Nanotechnology* **2005**, *16*, 350–353.
36. Stoller, M. D.; Park, S.; Zhu, Y.; An, J.; Ruoff, R. S. Graphene-Based Ultracapacitors. *Nano Lett.* **2008**, *8*, 3498–3502.
37. Zhu, Y.; Murali, S.; Stoller, M. D.; Ganesh, K. J.; Cai, W.; Ferreira, P. J.; Pirkle, A.; Wallace., R. M.; Cychosz, K. A.; Thommes, M.; *et al*. Carbon-Based Supercapacitors Produced by Activation of Graphene. *Science* **2011**, *332*, 1537–1541.
38. Gao, W.; Singh, N.; Song, L.; Liu, Z.; Reddy, A. L. M.; Ci, L.; Vajtai, R.; Zhang, Q.; Wei, B.; Ajayan, P. M. Direct Laser Writing of Micro-Supercapacitors on Hydrated Graphite Oxide Films. *Nat. Nanotechnol.* **2011**, *6*, 496–500.
39. Reddy, A. L. M.; Srivastava, A.; Gowda, S. R.; Gullapalli, H.; Dubey, M.; Ajayan, P. M. Synthesis of Nitrogen-Doped Graphene Films For Lithium Battery Application. *ACS Nano* **2010**, *4*, 6337–6342.
40. Gong, K.; Du, F.; Xia, Z.; Durstock, M.; Dai, L. Nitrogen-Doped Carbon Nanotube Arrays with High Electrocatalytic Activity for Oxygen Reduction. *Science* **2009**, *323*, 760–764.
41. Hata, K.; Futaba, D. N.; Mizuno, K.; Namai, T.; Yumura, M.; Lijima, S. Water-Assisted Highly Efficient Synthesis of Impurity-Free Single-Walled Carbon Nanotubes. *Science* **2004**, *306*, 1362–1364.
42. Datta, S. S.; Strachan, D. R.; Khamis, S. M.; Johnson, A. T. C. Crystallographic Etching of Few-Layer Graphene. *Nano Lett.* **2008**, *8*, 1912–1915.